# Product distributions and efficiencies for ethanol oxidation at PtNi octahedra

Rakan M. Altarawneh[a,b], Tobias M. Brueckner[a], Binyu Chen[a], and Peter G. Pickup[a]*

*a. Department of Chemistry, Memorial University, St. John's, Newfoundland, A1B 3X7, Canada*

*b. Department of Chemistry, Faculty of Science, Mu'tah University, Al-Karak, Jordan*

Journal of Power Sources 400 (2018) 369–376
https://doi.org/10.1016/j.jpowsour.2018.08.052

**Abstract**

An octahedral PtNi catalyst has been evaluated for direct ethanol fuel cells (DEFC) by measuring its performance and product distribution in a proton exchange membrane electrolysis cell. This avoids errors due to the chemical reaction between ethanol and oxygen that occurs in a DEFC. The performance of the PtNi/C catalyst at low potentials was similar to that of a commercial Pt/C catalyst, while its selectivity for complete oxidation of ethanol to carbon dioxide was significantly higher. For example, at 0.2 V vs. a hydrogen-producing cathode the faradaic yield of $CO_2$ was 73% at PtNi/C at an average current of 5.6 mA, but only 55% at Pt/C, at 5.1 mA. Consequently, the PtNi/C catalyst would provide higher DEFC efficiencies than Pt/C, or commercial PtRu/C. The voltammetric behaviors of PtNi/C and Pt/C have also been compared in a liquid electrolyte at ambient temperature, where it was found that the activity of the PtNi/C for ethanol oxidation was improved greatly by heating in acetic acid. This removes adsorbed Ni and capping agents and greatly improved CO tolerance. However, the superior CO tolerance of the cleaned PtNi/C relative to Pt/C was not reflected in polarization curves measured at 80 °C in PEM cells.

Keywords: ethanol oxidation, electrolysis, ethanol fuel cell; PtNi; efficiency; stoichiometry

**Corresponding author. Tel.: +1-709-864-8657; Fax: 1-709-864-3702; ppickup@mun.ca*

## 1. Introduction

Growing environmental concerns are driving the development of alternative kinds of renewable and clean energy sources with low $CO_2$ emissions. In this context, ethanol is one of the most important renewable energy sources because it is relatively safe, easily transported, and has a high energy density. It is widely used in gasoline, and can potentially be used more efficiently in fuel cells, either directly in direct ethanol fuel cells (DEFCs) or following reforming, or electrolysis, to produce hydrogen [1-4].

Nevertheless, the commercialization of DEFCs has been impeded by obstacles that need to be overcome such as the low current densities for the ethanol oxidation reaction, crossover of ethanol through the membrane, and low faradaic efficiencies [2, 3]. For efficient use of ethanol in DEFCs or ethanol electrolysis cells (EECs), it should be oxidized completely to carbon dioxide at the anode to generate 12 electrons ($n$ = 12), while oxygen is reduced to water at the cathode in a DEFC, or water is reduced to hydrogen in an EEC. However, the main products from DEFCs and EECs are acetaldehyde and acetic acid, which provide low faradaic efficiency because they only generate 2 and 4 electrons, respectively.

The anode catalysts most commonly used in DEFCs and EECs are based on platinum nanoparticles, which provide a high number of low coordination active sites and have relatively high selectivity for cleavage of the C–C bond of ethanol [5, 6]. Following adsorption on the active sites of Pt, the ethanol molecules can dissociate and oxidize to various species through a number of different pathways [7-9]. One path produces strongly adsorbed CO ($CO_{ad}$) and $CH_x$ intermediates, while other pathways lead to the formation of acetic acid and acetaldehyde. Further oxidation of adsorbed intermediate requires adsorbed OH species ($OH_{ad}$) to form $CO_2$. Consequently, adsorption of ethanol and cleavage of the C-C bond is inhibited by adsorbed intermediates, particularly $CO_{ad}$ at low overpotentials, and by excess $OH_{ad}$ at high overpotentials

[8]. Alloying or modification of Pt with oxophilic metals such as Ru and Sn improves its activity greatly, by formation of $OH_{ad}$ on the surface of the oxophilic metal at low overpotentials (bifunctional effect) and weakening the binding of $CO_{ad}$ by changing the electronic structure of the surface Pt atoms (electronic effect) [10]. However, measurements of product distributions have shown that the modification of Pt with Ru and/or Sn decreases the selectivity of the catalysts for complete oxidation of ethanol to $CO_2$ [5, 11].

Nickel has been shown to promote the catalytic activity of Pt for ethanol oxidation [12-18], and octahedral PtNi nanocrystals have been found to provide particularly high activities at ambient temperature [15]. *In situ* infrared spectroscopy showed that the poisoning effect of $CO_{ad}$ was significantly less at PtNi/C relative to Pt/C, although the acetic acid to $CO_2$ ratio was much higher. The aim of the work described here was to evaluate the performance and the selectivity of the reported octahedral PtNi/C alloy under conditions that would be experienced in a DEFC or EEC, at high temperature and with a polymer electrolyte. In particular, this work focusses on the stoichiometry, product distributions and efficiencies for ethanol oxidation at octahedral PtNi/C, and comparison with commercial Pt/C and PtRu/C catalysts. It is important to know whether Ni can increase the selectivity for C-C bond cleavage, like Rh [19, 20], or suppresses it like Ru and Sn.

## 2. Experimental

### *2.1. Chemicals and materials*

Carbon supported Pt (Pt/C; HiSPEC™ 13100, 70% Pt; Alfa Aesar), platinum acetylacetonate ($Pt(acac)_2$, 97%, Aldrich Chem. Co.), nickel acetylacetonate ($Ni(acac)_2$, 95%, Aldrich Chem. Co.), anhydrous ethanol (Commercial Alcohols Inc.), acetic acid (99.7%, Caledon Lab. Chemicals), oleylamine (70%, Aldrich Chem. Co.), oleic acid (90%, Aldrich Chem. Co.), benzyl ether (98%, Alfa Aesar), tungsten hexacarbonyl ($W(CO)_6$, 97%, Alfa Aesar), Nafion solution

(5%, DuPont) and carbon black (Vulcan XC-72, Cabot) were used as received. Nafion$^{TM}$ 115 and 117 membranes were pre-treated in 3% $H_2O_2$ for 1 h at 80 °C, 1 M sulfuric acid for 1 h at 80 °C, and deionized water for 3 h at 80 °C, and stored in deionized water.

*2.2. Synthesis of the PtNi/C catalyst*

A sample of the carbon supported PtNi (~30 mass%) catalyst was initially prepared following a literature procedure [15, 21]. A larger batch was then prepared by the same method as follows. 200 mg of $Pt(acac)_2$ and 100 mg of $Ni(acac)_2$ in 20 mL of oleylamine, 10 mL of oleic acid and 70 mL of benzyl ether were heated to 130 °C under $N_2$ protection with vigorous stirring. Then 600 mg of $W(CO)_6$ was rapidly added and the mixture was heated at 225°C for 40 min under $N_2$. Toluene (5 mL) and ethanol (15 mL) were added to the cooled solution followed by sonication for 5 min. The PtNi nanoparticles were isolated by centrifugation at 6000 rpm and then dispersed in toluene (10 mL) by sonication for 10 min. A carbon black suspension, prepared by sonication of 200 mg of carbon in toluene (5 mL) for 10 min, was added and the mixture was then sonicated for 3 h. The PtNi/C catalyst was collected by filtration, then stirred for 1 h in toluene, collected, and washed several times with toluene and ethanol. For further purification, batches of the PtNi/C catalyst were mixed with 20 mL of acetic acid and then heated at 60 °C for 2 or 4 h [21]. The suspensions were filtered, washed several times with ethanol and dried at 70 °C for 30 min.

*2.3. Physical characterization*

The crystal structure of the PtNi/C octahedral catalyst was investigated by using x-ray powder diffraction (XRD; Rigaku Ultima IV X-ray Diffractometer with a Cu $K_\alpha$ source and a scintillation counter detector). The composition was determined by thermal gravimetric analysis (TGA; TA Instruments Q500 TGA) and inductively coupled plasma - optical emission spectrometry (ICP-OES; Perkin-Elmer 5300 DV). Transmission electron microscopy (TEM) was

carried out at the University of New Brunswick (The Microscopy and Microanalysis Facility) with a JEOL 2011 200 keV scanning transmission electron microscope.

*2.4. Electrochemical measurements*

Cyclic voltammetry (CV) was performed in a conventional three-electrode glass cell controlled by a BioLogic SP-50 Potentiostat/Galvanostat. Catalyst coated glassy carbon disk working electrodes (0.071 $cm^2$) were prepared using suspensions of ca. 2 mg of PtNi/C or Pt/C catalyst in 120 μL of water, 30 μL of 2-propanol and 50 μL of 5% Nafion solution. Following sonication for 2 h, 3 μL of the catalyst suspension was pipetted onto a polished glassy carbon disk and allowed to dry overnight at ambient temperature. The catalyst loading was ca. 0.4 mg $cm^{-2}$ in all cases. The counter electrode was a platinum wire and the reference electrode was a saturated calomel electrode (SCE). All CV experiments were carried out in a $N_2$-purged 1.0 M sulfuric acid electrolyte at ambient temperature, and potentials are referred to SCE.

Before measurement of the ethanol oxidation activity, the working electrodes were cycled from -0.2 to 0.8 V at 100 mV $s^{-1}$ in 1 M $H_2SO_4$ for 3 cycles. Then each working electrode was cycled between -0.2 V and 0.8 V in 0.1 M ethanol + 1.0 M $H_2SO_4$ solution at a scan rate of 10 mV $s^{-1}$ for 3 cycles. The reported voltammograms are averages for the 2$^{nd}$ and 3$^{rd}$ cycles.

Measurements of catalyst activities at 80 °C were made initially in a proton exchange membrane (PEM) electrolysis cell with nine individual 0.236 $cm^2$ anodes, a Nafion 117 membrane, and a single 5 $cm^2$ Pt black cathode (Fig. S1), controlled with a MSTAT multi-channel potentiostat from Arbin Instruments [22]. Nine different channels were used to control the potentials of the anodes, with the counter and references leads for all channels connected to the single cathode. Anodes were prepared by spreading a suspension of the catalyst in a mixture of Nafion solution and 1-propanol onto Toray carbon fiber paper (CFP; TGP-H-090). The metal loading (Pt+Ni) was 3.2 mg $cm^{-2}$ and the Nafion loading was ca. 20 mass%. Two or three

electrodes prepared from each catalyst were used in order to assess the statistical significance of differences between catalysts. The cell was operated with 0.100 M ethanol supplied to the cathode at 0.2 or 0.5 mL $min^{-1}$ and $N_2$ was passed through the anode flow field at 30 mL $min^{-1}$ to exclude oxygen and collect $CO_2$. In this operating mode (crossover mode), ethanol crosses through the membrane to the anode (Fig. S1). This controls mass transport and provides information on the stoichiometry of the reaction [22]. Evolution of hydrogen at the cathode creates a dynamic hydrogen electrode (DHE) and provides a stable reference potential [23, 24]. The cell was preconditioned at 0.7 V for one hour at the operating temperature. Polarization curves were then obtained from 0.9 V to 0.0 V in 50 mV steps. The reported currents are averages over 120 s following a 60 s delay to allow the current to stabilize.

The use of 0.1 M ethanol in these experiments represents a compromise between electrochemical performance (power density) and faradiac efficiency (determined primarily by the $CO_2$ yield, which decreases with increasing ethanol concentration [25]). Data in the literature for $CO_2$ yields obtained with Pt/C catalysts covers ethanol concentrations from 0.01 M [25] to 2 M [26], and so we have selected an intermediate value for this and our previous work.

Product distributions, and the stoichiometry for ethanol oxidation, were measured in commercial PEM fuel cell hardware (Fuel Cell Technology Inc.) with 5 $cm^2$ electrodes and a Nafion 115 membrane [11]. The cell was operated with 0.100 M ethanol supplied to the anode at 0.2 or 0.5 mL $min^{-1}$ and $N_2$ was passed through the cathode flow field at 38 mL $min^{-1}$ to exclude oxygen and collect products [11]. The anode was prepared by mixing ca. 52 mg of PtNi/C catalyst, after treatment with acetic acid for 4 h, with ca. 260 μL of 5% Nafion and 200 μL of propanol, and sonication for 3 h at ambient temperature. The resulting suspension was spread onto CFP to give a metal (Pt+Ni) loading of 3.2 mg $cm^{-2}$ and a Nafion loading of ca. 20 mass%. The cathode consisted of 4 mg $cm^{-2}$ Pt black on CFP. Electrochemical measurements were made

under steady state conditions at constant cell potentials using a Hokuto Denko HA-301 potentiostat.

*2.5. Analysis of products and residual ethanol*

For analysis of the exhaust from the PEM cells, the $N_2$ and aqueous ethanol streams from the two flow fields were combined in a cold trap [11]. $CO_2$ in the $N_2$ leaving the trap was measured in real-time with a commercial non-dispersive infrared $CO_2$ monitor (Telaire 7001). Ethanol, acetic acid and acetaldehyde remaining in the trap were measured by using $^1$H NMR spectroscopy. $CO_2$ measurements were made, and samples were collected for NMR, while the cell was operating at steady-state at a constant potential and 80 °C, with 0.100 M ethanol solution at 0.2 mL $min^{-1}$.

**3. Results and discussion**

*3.1. Physical characterization of the PtNi/C catalyst*

The loadings of Pt and Ni based on ICP-OES for the as prepared PtNi/C bulk sample of the catalyst were 23.6% and 4.4% by mass, respectively. The Pt:Ni atomic ratio of 1.6 is the same as the literature value [21]. There was also a small amount of W (0.5%) from the $W(CO)_6$ employed in the synthesis. Heating the as prepared catalyst in acetic acid at 60 °C for 4 h increased Pt content to 24.9 mass% and decreased the Ni and W contents to 3.4% and 0.4%, respectively. The increase in the Pt:Ni atomic ratio to 2.2 is consistent with the previously reported preferential loss of Ni from the catalyst surface [21].

Alloy formation was confirmed by XRD, as shown in Fig. 1 where the peak positions of the as-prepared PtNi/C catalyst are compared with those for Pt and Ni from the International Centre for Diffraction Data. All of the diffraction peaks for the PtNi/C were between the corresponding peaks for Pt and Ni. The mean size of the PtNi particles was estimated to be 8.3 nm by applying the Scherrer equation to the Pt(111) peak, which is close to the average size of 9.0 nm reported

by Choi et al. [21]. Heating in acetic acid at 60 °C for 4 h produced only minor changes in the XRD, with small shifts to lower angles (Fig. S2) and a slight broadening, indicating a decrease in the average particle size to 8.0 nm. This is consistent with the loss of Ni indicated by the ICP-OES results.

The morphology of the PtNi/C catalyst was characterized by TEM (Fig. 1). It is clear from this image that the PtNi nanoparticles were relatively homogenous structures with a typically octahedral shape. The mean edge length of the PtNi nanoparticles was 9.0±1.0 nm (Fig. S3), which is in good agreement with the mean particles size obtained from XRD and reported in refs. [15, 21]. Since Choi et al. [21] have reported a detailed study of the TEM of octahedral PtNi particles prepared in the same way, our objective here was simply to confirm that we had prepared a similar catalyst. The shapes and defect/size distributions are very similar to those that have been previously reported [15, 21].

TGA (Figs. S4 and S5) showed a residual mass of 30.96% before treatment with acetic acid, which decreased slightly, to 30.62% and 30.30%, following treatment with acetic acid for 2 h and 4 h, respectively. This is consistent with the loss of surface Ni observed by ICP-OES [21]. The mass loss is due to adsorbed water and organic residue (oleylamine and oleic acid) and combustion of the carbon support. A mass loss of 1.4% at ca. 165 °C for the as prepared catalyst (Fig. S4) is consistent with the thermal decomposition and desorption of oleic acid [27], and was barely apparent following treatment with acetic acid (Fig. S5).

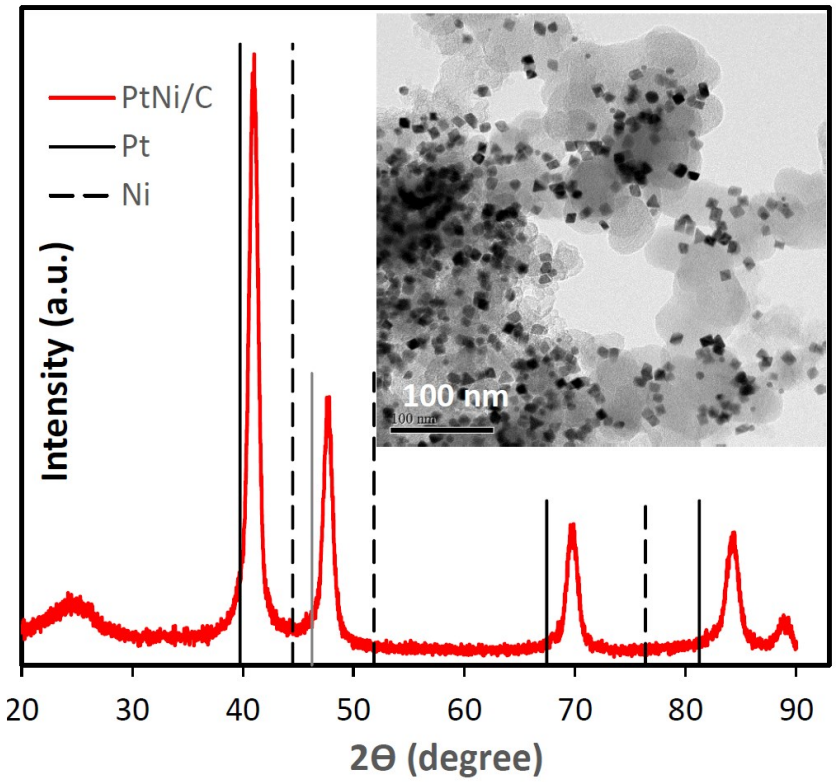


Fig. 1. X-ray diffraction pattern and TEM image (inset) of the as prepared bulk PtNi/C sample.

*3.2. Electrochemical measurements*

*3.2.1. Cyclic voltammetry*

Cyclic voltammograms for the PtNi/C catalyst before and after treatment with acetic acid and for a commercial Pt/C catalyst are shown in Fig. 2. The currents are normalized based on the mass of Pt, since the higher Pt content of the Pt/C produced higher Pt loadings for the same mass of catalyst. It is clear from this figure that the catalysts exhibit peaks with different areas in the hydrogen adsorption-desorption region from -0.20 V to 0.15 V. Electrochemically active areas determined from the charge under the H desorption peaks are shown in Table 1, together with the calculated geometric area based on the average particle size, and the percent utilization (active area/geometric area). It can be seen that the PtNi/C catalyst initially had a low active area and utilization relative to Pt/C.

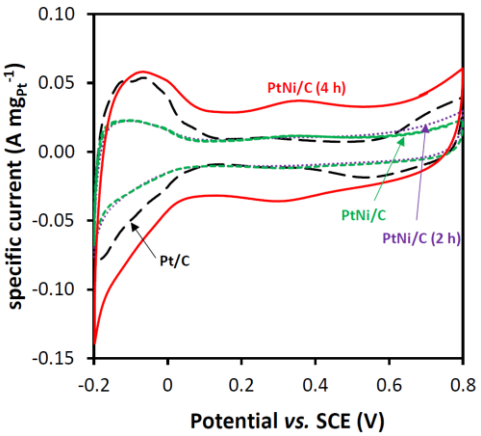


Fig. 2. Cyclic voltammograms (100 mV $s^{-1}$; 1 M $H_2SO_4$(aq)) of Pt/C (— —; 0.32 mg Pt $cm^{-2}$), the as prepared PtNi/C (····; 0.11 mg Pt $cm^{-2}$) and PtNi/C following treatment with acetic acid for 2 h (- - -; 0.10 mg Pt $cm^{-2}$) and 4 h (——; 0.11 mg Pt $cm^{-2}$).

Table 1. Surface areas and utilizations of the PtNi/C and Pt/C catalysts determined from the hydrogen desorption charges in Fig. 2.

| Catalyst | Geometric area ($cm^2$) | Electrochemical area ($cm^2$) | Utilization |
|---|---|---|---|
| Pt/C | 16 | 6.7 | 41% |
| as prepared PtNi/C | 4.4 | 0.60 | 13% |
| PtNi/C (2 h) | 4.0 | 0.66 | 16% |
| PtNi/C (4 h) | 4.1 | 1.2 | 30% |

We use have used Johnson Matthey Fuel Cell's 70% HiSPEC™ Pt/C catalyst here for comparison because it is the best commercial catalyst that we have found for ethanol oxidation, and therefore provides the most stringent test of new catalysts. We use the same mass loading of catalyst to achieve a compromise between Pt mass (higher for Pt/C than PtNi/C), and catalyst

layer thickness (lower for Pt/C). Using the same Pt mass would result in a large difference in thickness.

Heating in acetic acid for 2 h increased the utilization of the PtNi/C slightly, while 4 h treatment with acetic acid increased the utilization greatly. The lower utilization of PtNi/C relative to that for Pt/C is due in part to the presence of surface Ni. The increase in utilization with acetic acid treatment can be attributed to the removal of Ni from the Pt surface [21], and removal of residual capping agents (oleic acid and oleyl amine) from the synthesis. The greatly increased current in the double-layer region (0.15-0.4 V) when the PtNi/C was treated with acetic acid for 4 h is characteristic of the carbon support, and suggests that this was partially covered by residual organics for the as prepared sample.

Fig. 3 shows cyclic voltammograms for the PtNi/C and Pt/C catalysts in the presence of 0.1 M ethanol (in 1 M $H_2SO_4$(aq)). These voltammograms have been normalized based on the electrochemically active areas determined from the voltammograms in Fig. 2. On this basis, the PtNi/C catalyst was much more active for ethanol oxidation than Pt/C, as previously reported [15]. The much lower onset potential and higher peak currents at octahedral PtNi have been attributed to an electronic effect that weakens the Pt-CO bond [15], although it could also result from the bifunctional effect. The presence of an electronic effect is supported here by the observation that the charges in the hydrogen adsorption-desorption region in Fig. 3 are much higher for the PtNi/C catalyst than for the Pt/C catalyst. Since these voltammograms have been normalized based on the active areas measured in the absence of ethanol, this shows that a much lower fraction of the PtNi/C active area was blocked by CO and other strongly adsorbed intermediates.

Curiously, the ethanol oxidation peaks in Fig. 3 are highest for the as prepared PtNi/C catalyst, and decreased more with longer treatment with acetic acid. This is primarily an artifact of the

normalization, since differences in the peak currents in the reverse scan were not significant before normalization (Fig. S6). However, it does suggest that the species (Ni and/or organics) blocking the as-prepared PtNi/C were dissolved/desorbed during the ethanol oxidation experiments. Alternatively, these adsorbed species may enhance the current by inhibiting CO formation through the third-body effect.

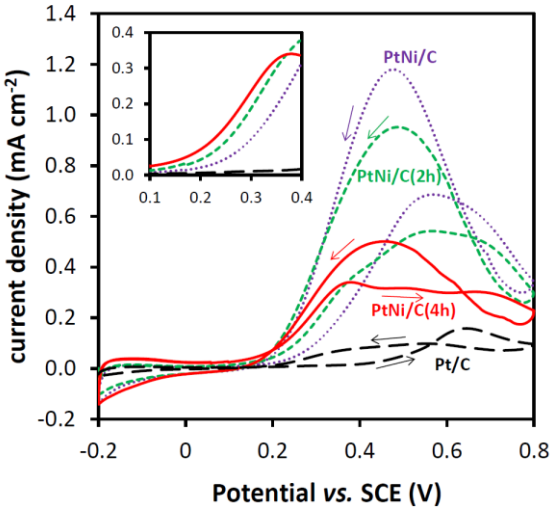


Fig. 3. Active area normalized cyclic voltammograms (10 $mVs^{-1}$), in 1 M $H_2SO_4$(aq) containing 0.1 M ethanol, at Pt/C (— —), the as prepared PtNi/C (····) and PtNi/C following treatment with acetic acid for 2 h (- - -) and 4 h (——). The inset shows an expansion of the 0.1 to 0.4 V region on the forward scan.

The most important effect of treatment of the PtNi/C catalyst with acetic acid was to shift the onset for ethanol oxidation to lower potentials. In Fig. 3, this is most notable after 2 h in acetic acid, while on a Pt mass basis the low potential performance of the sample treated for 4 h was much better.

*3.2.2. Ethanol electrolysis in a multi-anode PEM cell at 80* °C

A multi-anode PEM cell [22], operated at 80 °C, was used for preliminary evaluation of the PtNi/C catalyst for use in DEFCs and EECs, and for assessing the effects of treatment with acetic acid. This cell allows a number of catalysts to be tested and compared under the same conditions at the same time. Multiple electrodes prepared with each catalyst were used in order to assess the significance of differences between catalysts and to determine the reproducibility of the electrodes. All potentials reported in this section are versus the hydrogen evolving cathode (DHE). The cell was operated in crossover mode in order to control the diffusion of ethanol to the anode catalyst layer. In this mode, ethanol is pumped through the cathode flow field and diffuses through the membrane to the anode, which is purged with $N_2$ (Fig. S1) The current is mass transport controlled at high potentials ($i_{mt}$), and is therefore proportional to the average number of electrons transferred ($n_{av}$) (eq. 1) [22].

$$i_{mt} = n_{av}FmC \qquad (1)$$

where $m$ is the mass transport coefficient (independent of potential and time) and $C$ is the bulk concentration of ethanol.

Fig. 4 shows polarization curves for the oxidation of 0.1 M ethanol at PtNi/C and Pt/C anodes. Two different samples of the PtNi/C catalyst were used; an as prepared sample from the first batch (small scale synthesis), and a sample from the second batch that had been heated in acetic acid for 4 h (PtNi/C(4 h)). It can be seen from Fig. 4 that there were no significant differences between the currents at the two PtNi/C anodes, indicating that acetic acid treatment did not affect the catalytic activity at 80 °C in the PEM cell. This observation indicates that the species that blocked the Pt surface in the CV experiments were largely removed during start-up and conditioning of the PEM cell.

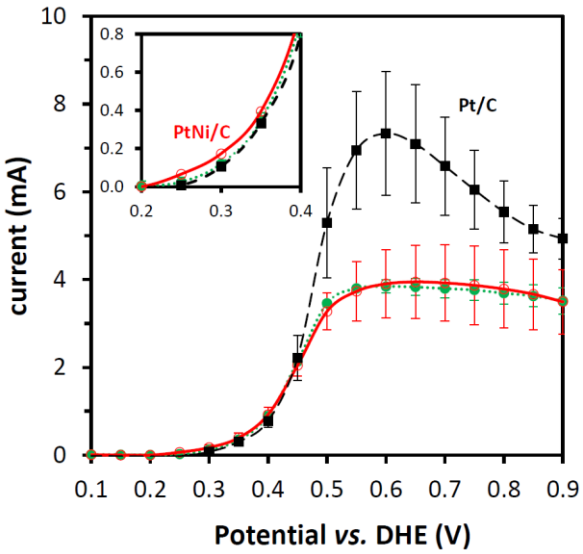


Fig. 4. Steady-state polarization curves for the oxidation of 0.100 M ethanol (0.5 mL $min^{-1}$) at 80 ºC in a nine-anode PEM cell in crossover mode at as-prepared PtNi/C (····; 3 anodes; 3.2 mg $cm^{-2}$ PtNi), PtNi/C following treatment with acetic acid for 4 h (——; 2 anodes; 3.2 mg $cm^{-2}$ PtNi), and Pt/C (— —; 3 anodes; 3.2 mg $cm^{-2}$ Pt). Averages and standard deviations for the multiple anodes of each catalyst are shown. The inset shows an enlargement of the onset region.

In comparison with Pt/C, the currents at the PtNi/C anodes were not significantly different at potential up to 0.45 V, but were significantly lower at higher potentials. Since this is the diffusion limited region, it indicates that at potentials > 0.45 V fewer electrons were transferred per ethanol molecule at PtNi/C relative to Pt/C. This is consistent with an *in situ* FTIR study at ambient temperature which showed that the acetic acid to $CO_2$ ratio was much higher at octahedral PtNi/C than at Pt/C. Since production of acetic acid involves transfer of 4 electrons, while formation of $CO_2$ requires 12 electrons to be transferred, $n_{av}$ decreases as the acetic acid to $CO_2$ ratio increases (eq. 2).

$$n_{av} = \sum n_i f_i \qquad (2)$$

where $n_i$ is the number of electrons transferred to form product $i$ and $f_i$ is the fraction of ethanol converted to product $i$.

The decreasing current for the Pt/C catalyst at high potentials in Fig. 4 is due to a decrease in $n_{av}$ [22] due to an increasing acetic acid to $CO_2$ ratio [11]. Consequently, the almost constant current in this region for the PtNi/C catalyst indicates that the $CO_2$ yield and acetic acid to $CO_2$ ratio did not change significantly with potential.

Comparison of the results in Fig. 4 with those in Fig. 3, for ethanol oxidation in $H_2SO_4$(aq) at ambient temperature, reveals stark differences. In particular, the shift in onset potential seen in the aqueous electrolyte at ambient temperature is much weaker in the PEM cell at 80 °C. This can be attributed largely to the effects of temperature on the oxidation of adsorbed CO at Pt, which shifts to lower potentials with increasing temperature [28]. Since PtNi is less susceptible to CO poisoning during ethanol oxidation [15], increasing the temperature would be expected to have a smaller effect on the onset of CO oxidation, as reported for PtRu [28]. If the onset of sustained ethanol oxidation is determined by the coverage of adsorbed CO, this could explain the smaller difference in onset potentials at 80 °C. Support for this hypothesis can be found in Fig. 3 if the positions of the peak at ca. 0.4 V on the reverse scans are compared. Here, the coverage of CO is low because the oxide layer on the Pt surface has just be reduced [29], and consequently there are not significant differences in the position of this peak.

Comparison of peak currents between Figs. 3 and 4 would not be meaningful because the conditions were so different. Also, the currents in Fig. 4 have not been normalized because the purpose of the experiments in the nine-anode cell was to observe onset potentials, determine mass transport limited currents, and make a preliminary assessment of the stability of the PtNi/C catalyst under DEFC conditions. In addition, it was expected from previous work that there

would not be a significant dependence on the loading of Pt, or Pt surface area [22] (i.e. that employing thicker catalyst layers would not have significantly increased the currents).

The nine-anode cell was also used, for first time, to measure the efficiency for the complete oxidation of ethanol, by passing the $N_2$ from the cell exhaust though a NDIR $CO_2$ monitor. Fig. 5 shows current and $CO_2$ concentration traces recorded over 500 s at 0.5 V. In these experiments the anodes of each type (2 or 3) were run in groups to increase the $CO_2$ reading and provide an average value for each catalyst. The relatively stable $CO_2$ readings, once the concentration in the liquid trap had equilibrated, demonstrate that the nine-anode cell is suitable for $CO_2$ measurements. The average faradaic $CO_2$ yield was 79% for the Pt/C catalyst, which is close to the value of 75% previously reported for this catalyst under similar conditions in a 5 $cm^2$ single anode cell. The average $CO_2$ yields for the PtNi/C anodes were significantly lower than this at 21% (one measurement) for the as-prepared catalyst and 28.8±1.6% (average and standard deviation for 3 runs) following heating in acetic acid. This is consistent with the much lower $n_{av}$ values indicated by the mass transport limited currents in Fig. 4.

The higher $CO_2$ yield for the sample treated with acetic acid suggests that the selectivity of the PtNi/C is more sensitive to the surface coverage of Ni and/or organic species than the current. Interestingly, the as-prepared catalyst gave a higher average current in these experiments, suggesting again that there may have been a third body effect. The lower $CO_2$ yield implies that $CO_{ad}$ was formed more slowly, which would be expected if more Pt sites were occupied by Ni and/or organic species.

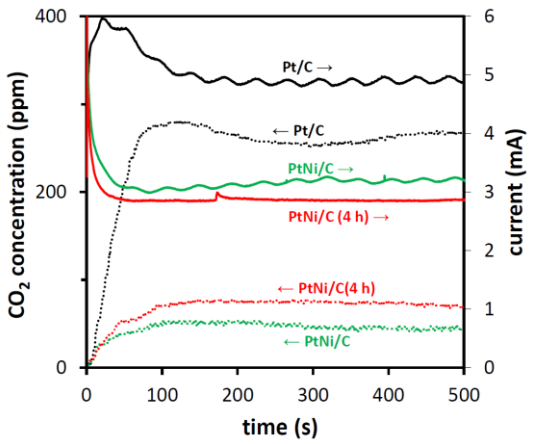


Fig. 5. Currents (solid lines) and $CO_2$ concentrations (dotted lines) for the oxidation of 0.100 M ethanol (0.2 mL $min^{-1}$) at 0.5 V and 80 ºC at PtNi/C and Pt/C anodes in a nine-anode PEM cell operating in crossover mode.

*3.2.3. Ethanol electrolysis in a 5 $cm^2$ PEM cell at 80 °C*

A sample of the PtNi/C catalyst that had been heated at 60 °C in acetic acid for 4 h was tested in a PEM cell with a 5 $cm^2$ anode in order to determine the product distribution and stoichiometry of ethanol oxidation. Use of a larger anode increases the consumption of ethanol and the concentrations of products, which is necessary to achieve good accuracy and mass balance. Otherwise, small losses of ethanol and products from the cell and exhaust can cause large errors and uncertainties. The cell was operated with 0.1 M ethanol passing through the anodes flow field and $N_2$ passing through the cathode flow field (anode polarization mode [30]). This emulates the conditions at the anode of a DEFC while avoiding errors due to the chemical reaction of oxygen with ethanol that occurs in a DEFC [31-33]. Errors due to the crossover of ethanol and products to the cathode [31] were avoided by combining the anode and cathode exhausts prior to analysis [11].

Fig. 6 shows polarization curves for the oxidation of 0.1 M ethanol at PtNi/C and Pt/C and anodes. Data for Pt/C has been previously published and discussed [11]. The PtNi/C and Pt/C

catalysts had similar onset potentials for ethanol oxidation, with slightly higher currents at PtNi/C relative up to 0.4 V, while at higher potentials PtNi/C showed lower currents than Pt/C. This is consistent with the results in Fig. 4 for smaller anodes, although quantitative comparisons are difficult because of the different modes of operation of the cells. As for the nine-anode PEM cell, the polarization curves in the single anode cell do not show the significant difference in onset potential between PtNi/C and Pt/C that would have been predicted from cyclic voltammetry.

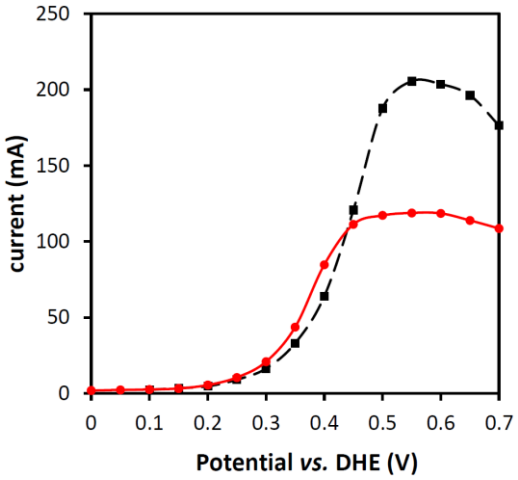


Fig. 6. Steady-state polarization curves for the oxidation of 0.100 M ethanol (0.5 mL $min^{-1}$) at 80 ºC in a 5 $cm^2$ PEM cell in anode polarization mode, with PtNi/C (4 h) (——; 3.2 mg $cm^{-2}$ PtNi) and Pt/C (— —; 3.2 mg $cm^{-2}$ Pt) anodes.

Fig. 7 shows the product distribution as a function of potential for the PtNi/C (4 h) electrode. The data is reported here as chemical yields, which are most useful for assessing the stoichiometry and efficiency. However, to facilitate comparison with the results from Fig. 5 and many literature reports, the discussion below uses both chemical and faradiac yields.

The results in Fig. 7 confirm the conclusions from the experiments in the nine-anode PEM cell that $CO_2$ yields are low for the PtNi/C catalyst at high potentials, and that the stoichiometry ($n_{av}$) for ethanol oxidation is low. From 0.5 to 0.7 V, 79-87% of the ethanol consumed was oxidized to acetic acid, only 10-16% was oxidized to $CO_2$, and only 1-2% was converted to acetaldehyde. Compared with Pt/C, PtNi/C is much less effective for the complete oxidation of ethanol over this potential range [11]. Its selectivity is similar to that for PtRu/C, which produced 90-93% acetic acid, ca. 4% $CO_2$ , and 4-7% acetaldehyde under these condition [11].

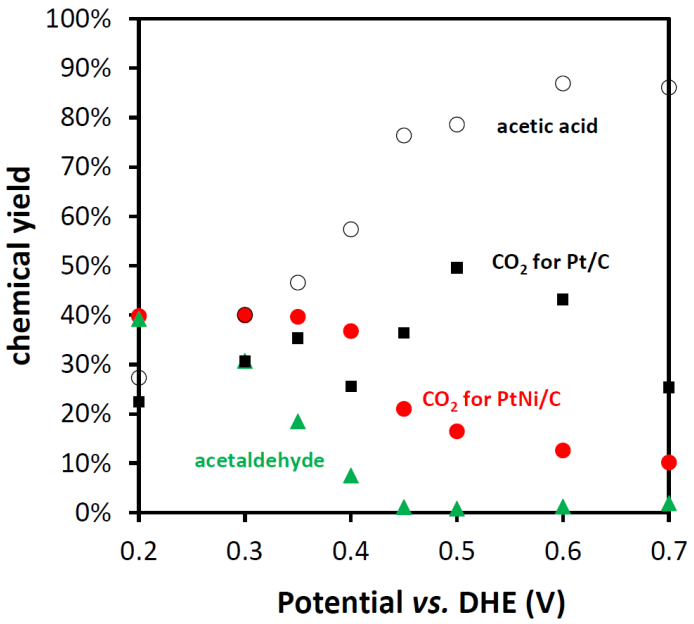


Fig. 7. Chemical yields of $CO_2$ (●), acetic acid (○), and acetaldehyde (▲) as a function of potential for oxidation of 0.100 M ethanol (0.2 mL $min^{-1}$) at a PtNi/C (4h) anode in a 5 $cm^2$ PEM cell at 80 °C. $CO_2$ yields for 70% Pt/C (■) from ref. [11] are shown for comparison.

At lower potentials, the product distribution from the PtNi/C anode was very different, and unexpected. The $CO_2$ yield rose sharply as the potential was decreased from 0.5 V to 0.4 V, reaching a plateau of 40% between 0.2 and 0.35 V. This chemical yield corresponds to a faradaic yield of ca. 70%, and is only rivalled by a few results in the literature [11, 25, 34-38]. Except for

one report on PtRu at an unsustainable high temperature of 145 °C [34], faradaic $CO_2$ yields above 50% have only been observed with pure Pt catalysts. Notably, the PtNi/C catalyst employed here produced higher $CO_2$ yields than the 70% Pt/C catalyst [11] from 0.2 to 0.4 V (Fig. 7), which corresponds to the approximate operating range of the anode in a DEFC [24]. In particular, at 0.2 V the faradaic yield of $CO_2$ was 73% at the PtNi/C anode at an average current of 5.6 mA, but only 55% at the 70% Pt/C anode, at 5.1 mA.

The higher selectivity for $CO_2$ at the PtNi/C catalyst at low potentials is difficult to explain, since it is so unusual, and contrary to measurements that have been reported for the same catalyst at ambient temperature in a liquid electrolyte [15]. In that work, the onset of $CO_2$ formation did not begin until ca. 0.55 V vs. RHE, which was the same onset potential observed for Pt/C. The observation of large $CO_2$ yields at potentials as low as 0.2 V vs. DHE in this work can be attributed primarily to the higher temperature employed, which promotes both C-C bond cleavage and $CO_{ad}$ oxidation at Pt. The presence of Ni on the Pt surface would be expected to promote CO oxidation at low potentials [39], which should increase the current, as observed for PtRu/C [11]. However, the currents observed at PtNi/C and Pt/C were similar in the two polarization curves (Fig. 6), and during product analysis. Furthermore, PtRu/C produces much lower yields of $CO_2$ than Pt/C: the chemical yield of $CO_2$ at a PtRu/C anode increased from 2% at 0.2 V to a maximum of 7% at 0.4 V under the conditions employed here [11]. It is clear therefore that the effect of Ni is very different to the effect of Ru. Since Ru is thought to promote ethanol oxidation primarily through the bi-functional effect (Ru-OH promotes Pt-CO oxidation), this suggests that the promotion of C-C bond cleavage by Ni may be due to an electronic effect. Indeed, electron transfer from Ni to Pt in a PtNi catalyst has been observed by X-ray photoelectron spectroscopy to be more pronounced than for PtRu [39].

Another factor that is likely to be important here is the solubility of Ni in acid. Heating of the PtNi/C catalyst in acetic acid for 4 h presumably removed most of the surface Ni atoms [21], and residual surface Ni may have been dissolved by the Nafion electrolyte during operation of the PEM cell. This would reduce or eliminate the effect of surface Ni-OH, which would mainly produce acetic acid at low potentials [8, 10]. However, the electronic effect of sub-surface Ni would persist, and the high percentage of surface Pt atoms would promote C-C cleavage by providing a high density of suitable Pt atom ensembles [40].

Although the $CO_2$ yield is the main factor that determines the faradaic efficiency of a DEFC, determining the full product distribution is important from an emissions perspective, and for accurately determining the efficiency. The overall efficiency of a DEFC ($\varepsilon_{DEFC}$) is given by eq. 3 [2]:

$$\varepsilon_{DEFC} = \varepsilon_{rev}\, \varepsilon_E\, \varepsilon_F \qquad (3)$$

where $\varepsilon_{rev}$ is the theoretical efficiency of 96% at 80 °C, $\varepsilon_E$ is the potential efficiency ($\varepsilon_E = E_{cell}/E_{rev}$, where $E_{rev}$ is the reversible cell potential of ca. 1.15 V), and $\varepsilon_F$ is the faradaic efficiency ($\varepsilon_F = n_{av}/12$). Consequently, a full evaluation of a catalyst for use in DEFCs requires determination of $n_{av}$ as a function of cell potential. It was determined here from the product distribution by using eq. 2, and the accuracy of the results was confirmed by comparison with values determined from the amount of ethanol consumed and from the faradaic yields, as previously described [38]. Averages and standard deviation from the three methods are reported in Table 2.

At low potentials (≤ 0.4 V), more electrons were transferred per ethanol molecule at PtNi/C than at either Pt/C or PtRu/C, meaning that the faradaic efficiency in a DEFC would be higher. Although the highest $n_{av}$ of 7.86 was observed at Pt/C, this was at an anode potential of 0.5 V,

which is not useful in a DEFC. However, the maximum $n_{av}$ of 6.90 for PtNi/C was at 0.35 V, which would provide a higher potential efficiency in a DEFC. Although PtRu/C is a much better catalyst than either Pt/C or PtNi/C in terms of current and power densities at low potentials, its maximum $n_{av}$ was only 4.50 at 0.5 V, which would lead to a low overall efficiency [11].

Table 2. $n_{av}$ vs. potential for the oxidation of 0.100 M ethanol (0.2 mL $min^{-1}$; 80 °C) at PtNi/C, Pt/C and PtRu/C anodes.

| Potential (V) | PtNi/C (4 h) | 70% Pt/C [11] | 75% PtRu/C [11] |
|---|---|---|---|
| 0.20 | 6.54±0.01 | 4.75±0.20 | 3.14±0.15 |
| 0.30 | 6.80±0.01 | 5.68±0.15 | 3.93±0.09 |
| 0.35 | 6.89±0.13 | 6.14±0.04 | 4.19±0.11 |
| 0.40 | 6.79±0.03 | 5.38±0.15 | 4.37±0.10 |
| 0.45 | 5.63±0.06 | 6.60±0.15 | 4.42±0.14 |
| 0.50 | 5.23±0.01 | 7.86±0.15 | 4.50±0.07 |
| 0.60 | 5.00±0.08 | 7.39±0.10 | 4.31±0.18 |
| 0.70 | 4.73±0.03 | 5.98±0.06 | 4.14±0.16 |

It should be noted that the $n_{av}$ values reported in Table 2 were measured in an EEC, since measurements in a DEFC would be inaccurate due to the chemical reaction that occurs between oxygen and ethanol [31]. However, the EEC potentials are not the same as DEFC potentials, and so cannot be used directly to determine $\varepsilon_{DEFC}$ by using eq. 3. However, they can be used to estimate $E_{cell}$ for a DEFC by using a typical set of cathode potential, as previously described [11]. Fig. 8 shows overall DEFC efficiencies vs. power density that have been calculated in this way from the data in Table 2. It can be seen that the PtNi/C catalyst would provide significantly higher efficiencies than Pt/C, except at the highest power densities, and higher efficiencies than

PtRu/C at all power densities. An important observation here is that the much higher electrochemical performance of PtRu/C (compare the power densities at 0.2 V in Fig. 8) comes at the expense of efficiency, which is very low (≤ 12.2%) at all potentials. These results indicate that the selectivity of the catalyst has a vital effect on its efficiency.

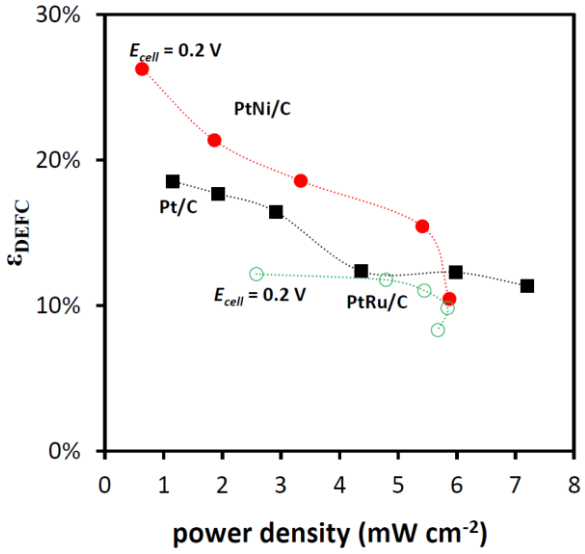


Fig. 8. Predicted efficiency vs. power density for DEFCs operating with 0.100 M ethanol at 80 °C with PtNi/C (●), Pt/C (■), and PtRu/C (○) anodes.

It should be noted that the power densities in Fig. 8 are low compared with typical values reported for DEFCs [2]. This is primarily due to the low ethanol concentration that was employed. Use of higher ethanol concentrations increases the power density, but decreases the $CO_2$ yield [25, 35], and therefore decreases the faradaic efficiency. In addition the cathode potentials [11, 24] employed in the calculation of the power and efficiency here are underestimates of the current state of the art. A better cathode would improve both the power and efficiency, and consequently increase the superiority of the PtNi/C catalyst over the Pt/C and PtRu/C catalysts, because the faradaic efficiency would become a more important factor.

From a practical perspective, the efficiencies and power densities reported for the PtNi/C catalyst in Fig. 8 are still too low, and the production of acetaldehyde at low anode potentials is too high. However, there are a number of approaches available to develop high performance DEFCs based in this octahedral PtNi catalyst. In addition to increasing the cathode performance, the PtNi can be modified with Rh to improve its low potential performance and selectivity for $CO_2$ [17], potential modulation can be employed to periodically strip $CO_{ad}$ [41, 42], and oxide supports can be used to enhance performance [43, 44]. Production of acetaldehyde, which greatly decreases the faradaic efficiency and is harmful, can be mitigated by using catalyst mixtures, and/or bilayer anodes [45].

**4. Conclusions**

Although PtNi octahedra show greatly enhanced activity for ethanol oxidation at ambient temperature in aqueous acid electrolytes ($HClO_4$ in [15] and $H_2SO_4$ here), this effect is not seen at 80 °C in a PEM cell. Instead, the differences between PtNi octahedra and commercial Pt nanoparticles in a PEM cell are more subtle, and potentially more important. At low potentials, there are no significant differences between the electrochemical performances (current and power density) of the two types of catalyst, but the PtNi octahedra are more selective for breaking the C-C bond of ethanol to produce $CO_2$. This increases the average number of electrons transferred and the faradaic efficiency. In a direct ethanol fuel cell, this would produce a significant increase in the overall efficiency. The importance of this result rests in the observations that the stoichiometry ($n_{av}$) of ethanol oxidation at low anode potentials is the most important factor influencing the efficiency of a DEFC, and that a high degree of conversion of ethanol to $CO_2$ is necessary in almost all applications. This demonstrates that studies in a PEM electrolysis or fuel cell, and quantitative product analysis, are crucial for evaluation of new catalysts, and for developing catalysts that will facilitate the commercialization of DEFCs.

The activity and $CO_2$ yield of the PtNi octahedra are sensitive to the presence of surface Ni and/or capping agents (oleylamine and oleic acid). In $H_2SO_4$, cyclic voltammetry showed a large increase in active Pt area following heating of the catalyst in acetic acid at 60 °C, and a large decrease in CO poisoning during ethanol oxidation. In contrast, cleaning of the Pt surface in this way decreased the electrochemical performance of the PtNi in the PEM cell slightly, but increased the yield of $CO_2$. This suggests that Ni, oleylamine and/or oleic acid at the Pt surface can play a number of roles (e.g. bifunctional, electronic, third-body) in determining activity and selectivity, and warrants further investigation.

**Funding:** This work was supported by the Natural Sciences and Engineering Research Council of Canada [grant number 2017-04260] and Memorial University.

**References**

[1] S.P.S. Badwal, S. Giddey, A. Kulkarni, J. Goel, S. Basu, Applied Energy, 145 (2015) 80-103.

[2] L. An, T.S. Zhao, Y.S. Li, Renew. Sustain. Energy Rev., 50 (2015) 1462-1468.

[3] B.C. Ong, S.K. Kamarudin, S. Basri, Int. J. Hydrogen Energy, 42 (2017) 10142-10157.

[4] C. Lamy, T. Jaubert, S. Baranton, C. Coutanceau, J. Power Sources, 245 (2014) 927-936.

[5] J. Friedl, U. Stimming, Electrochim. Acta, 101 (2013) 41-58.

[6] M.A.F. Akhairi, S.K. Kamarudin, Int. J. Hydrogen Energy, 41 (2016) 4214-4228.

[7] H.F. Wang, Z.P. Liu, J. Am. Chem. Soc., 130 (2008) 10996-11004.

[8] R. Kavanagh, X.M. Cao, W.F. Lin, C. Hardacre, P. Hu, Angew. Chem. Int. Ed. Engl., 51 (2012) 1572-1575.

[9] J. Florez-Montano, G. Garcia, O. Guillen-Villafuerte, J.L. Rodriguez, G.A. Planes, E. Pastor, Electrochim. Acta, 209 (2016) 121-131.

[10] J.M. Jin, T. Sheng, X. Lin, R. Kavanagh, P. Hamer, P.J. Hu, C. Hardacre, A. Martinez-Bonastre, J. Sharman, D. Thompsett, W.F. Lin, Phys. Chem. Chem. Phys., 16 (2014) 9432-9440.

[11] R.M. Altarawneh, P.G. Pickup, J. Electrochem. Soc., 164 (2017) F861-F865.

[12] V. Comignani, J.M. Sieben, M.E. Brigante, M.M.E. Duarte, J. Power Sources, 278 (2015) 119-127.

[13] A.B. Kuriganova, D.V. Leontyeva, S. Ivanov, A. Bund, N.V. Smirnova, J. Appl. Electrochem., 46 (2016) 1245-1260.

[14] E. Antolini, Energies, 10 (2017) 42.

[15] J.E. Sulaiman, S.Q. Zhu, Z.L. Xiang, Q.W. Chang, M.H. Shao, ACS Catalysis, 7 (2017) 5134-5141.

[16] S. Beyhan, J.M. Leger, F. Kadirgan, Appl. Catal. B Environ, 144 (2014) 66.

[17] N. Erini, V. Beermann, M. Gocyla, M. Gliech, M. Heggen, R.E. Dunin-Borkowski, P. Strasser, Angew. Chem. Int. Ed., 56 (2017) 6533-6538.

[18] S. Beyhan, J.M. Leger, F. Kadirgan, Appl. Catal., B Env., 130 (2013) 305-313.

[19] K. Bergamaski, E.R. Gonzalez, F.C. Nart, Electrochim. Acta, 53 (2008) 4396-4406.

[20] A.B. Delpeuch, T. Asset, M. Chatenet, C. Cremers, J. Electrochem. Soc., 161 (2014) F918-F924.

[21] S.I. Choi, S.F. Xie, M.H. Shao, J.H. Odell, N. Lu, H.C. Peng, L. Protsailo, S. Guerrero, J.H. Park, X.H. Xia, J.G. Wang, M.J. Kim, Y.N. Xia, Nano Lett., 13 (2013) 3420-3425.

[22] T.M. Brueckner, P.G. Pickup, J. Electrochem. Soc., 64 (2017) F1172-F1178.

[23] X. Ren, T.E. Springer, S. Gottesfeld, J. Electrochem. Soc, 147 (2000) 92-98.

[24] G. Li, P.G. Pickup, J. Power Sources, 161 (2006) 256-263.

[25] S. Sun, M.C. Halseid, M. Heinen, Z. Jusys, R.J. Behm, J. Power Sources, 190 (2009) 2-13.

[26] S. Rousseau, C. Coutanceau, C. Lamy, J.M. Leger, J. Power Sources, 158 (2006) 18-24.

[27] V. Perez-Dieste, O.M. Castellini, J.N. Crain, M.A. Eriksson, A. Kirakosian, J.L. Lin, J.L. McChesney, F.J. Himpsel, C.T. Black, C.B. Murray, Appl. Phys. Lett., 83 (2003) 5053-5055.

[28] T. Kawaguchi, W. Sugimoto, Y. Murakami, Y. Takasu, Electrochem. Commun., 6 (2004) 480-483.

[29] Y.Z. Zhao, X.M. Li, J.M. Schechter, Y.A. Yang, RSC Advances, 6 (2016) 5384-5390.

[30] P. Majidi, R.M. Altarawneh, N.D.W. Ryan, P.G. Pickup, Electrochim. Acta, 199 (2016) 210-217.

[31] D.D. James, P.G. Pickup, Electrochim. Acta, 55 (2010) 3824-3829.

[32] A. Jablonski, P.J. Kulesza, A. Lewera, J. Power Sources, 196 (2011) 4714–4718.

[33] A. Jablonski, A. Lewera, Appl. Catal. B Environ, 115 (2012) 25-30.

[34] A.S. Arico, P. Creti, P.L. Antonucci, V. Antonucci, Electrochem. Solid. State. Lett, 1 (1998) 66-68.

[35] D.D. James, P.G. Pickup, Electrochim. Acta, 78 (2012) 274-278.

[36] N. Nakagawa, Y. Kaneda, M. Wagatsuma, T. Tsujiguchi, J. Power Sources, 199 (2012) 103-109.

[37] J. Seweryn, A. Lewera, Appl. Catal. B Environ, 144 (2014) 129-134.

[38] R.M. Altarawneh, P. Majidi, P.G. Pickup, J. Power Sources, 351 (2017) 106-114.

[39] K.W. Park, J.H. Choi, B.K. Kwon, S.A. Lee, Y.E. Sung, H.Y. Ha, S.A. Hong, H. Kim, A. Wieckowski, J. Phys. Chem. B, 106 (2002) 1869-1877.

[40] S.E. Evarts, I. Kendrick, B.L. Wallstrom, T. Mion, M. Abedi, N. Dimakis, E.S. Smotkin, ACS Catalysis, 2 (2012) 701-707.

[41] P. Majidi, P.G. Pickup, J. Power Sources, 268 (2014) 439-442.

[42] A. Jablonski, A. Lewera, Chinese Journal of Catalysis, 36 (2015) 496-501.

[43] N.R. Elezovic, V.R. Radmilovic, N.V. Krstajic, RCS Advances, 6 (2016) 6788-6801.

[44] G.M. Alvarenga, H.M. Villullas, Current Opinion in Electrochemistry, 4 (2017) 39-44.

[45] R.M. Altarawneh, P.G. Pickup, J. Power Sources, 366 (2017) 27-32.